ISSN (ONLINE): 2454-9762
ISSN (PRINT): 2454-9762
Available online at www.ijarmate.com

International Journal of Advanced Research in Management, Architecture, Technology and Engineering (IJARMATE)
Vol. 8, Issue 7, July 2022

A NEW DESIGN OF ENERGY EFFICIENT HIGH-POWER PARTIAL RESONANCE MATRIX CONVERTER FOR FUTURE HYBRID AIRCRAFT

MONISHA A

M.E. Power Electronics and Drives

Marthandam College of Engineering & Technology

Kuttakuzhi, Marthandam

monishakrishnan27@gmail.com

Mr. G. W. MARTIN

Associate Professor

Department of EEE

Marthandam College of Engineering & Technology

Marthandam, macet.office@gmail.com

Abstract*— The paper analyzes and simulates the performance of an energy-efficient PWM modulation strategy designed for squirrel cage induction motor drive based on the partial resonance inverter (PRI). With hybrid electric aircraft (HEA), both propelling and auxiliary power can be electrified, thus pushing the limits of electrification. An input power converter with unity power at the input is a reliable, efficient, and compact configuration. Each cycle of the converter is only partially resonant, i.e. only a small time interval is allotted to resonance. Partially resonance inverters (PRIs) are compact due to their high frequency of operation. A soft switch allows for higher switching frequency, reducing passive component size due to the high frequency of the link and the soft switch allows for higher switching frequency. Matrix converters convert energy from three-phase sources to drive squirrel cage induction motors and electrically propelled fans directly on the aircraft. In this survey, we examine the influence of these concerns, present challenges and opportunities, and provide a glimpse of the future of technology. Keywords—HEA(Hybrid electric aircraft) PRI (Partial Resonance Inverter) (key words)

I. INTRODUCTION

Global emissions are primarily caused by the transport sector, according to the survey. Passenger cars and freight transportation are responsible for this. Emissions from conventional engines are high, and these emissions can cause a number of health problems, and in turn have a detrimental effect on human health. In order to reach emission-free transport, it is necessary to use the advanced technologies that promote emission-free technology. PHEVs (plug-in hybrid electric vehicles) are currently used in place of HEVs (hybrid electric vehicles). High Frequency link power converters can be used as an alternative to more traditional DC link power converters. An individual load or source can be modified according to their particular voltage requirements using a high frequency ac voltage link. The system can be made small by operating the link at a high frequency due to the considerable reduction in the size of passive components needed for filtering and temporary energy storage. High frequency operation also improves system response time and lowers acoustic noise if the frequency is above the audible range. Dc voltage or current links are commonly used in variable frequency drives to distribute power between the input and output converters and to temporarily store energy.

There are various inherent limits to dc link-based power conversion systems. Voltage dc link converters include bulky electrolytic capacitors, which severely reduce power converter reliability. The large switching loss and device stress that occur during switching intervals are another significant constraint of dc link converters. The practical switching frequencies are drastically lowered as a result of this. Furthermore, while the basic voltage sourced PWM drive's cost, size, and weight seem appealing, problems with input harmonics, output dV/dt and overvoltage, EMI/RFI, tripping with voltage sags, and other issues greatly reduce the drive's economic competitiveness. To minimise these issues, add-ons are available, but they may double or triple total costs and losses, as well as result in significant increases in volume and weight. As a better option, partial resonant converters classed as high frequency ac link converters have been proposed .Furthermore, the load as well as parasitic inductance and capacitance have a significant impact on the performance of resonant ac ac converters.

The last type is a matrix converter, which is the most adaptable because the output frequency and amplitude are unrestricted. It uses a matrix of semiconductor bidirectional switches, with a switch connected between each input terminal and each output terminal, to replace several conversion stages and thus the intermediate energy storage element, and it uses a single power conversion stage. The proposed topology is supposed to provide compactness, increased dependability, and

ISSN (ONLINE): 2454-9762
ISSN (PRINT): 2454-9762
Available online at www.ijarmate.com

International Journal of Advanced Research in Management, Architecture, Technology and Engineering (IJARMATE)
Vol. 8, Issue 7, July 2022

efficiency.

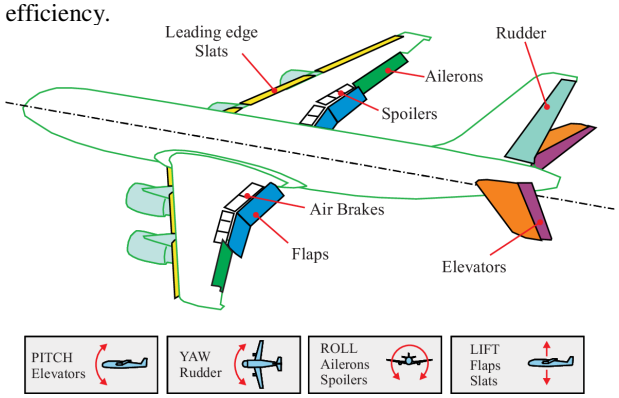

Fig 1 Electric Aircraft

II. HYBRID-ELECTRIC ARCHITECTURES

THREE MAIN POWER ARCHITECTURES:

There are three basic power designs for a hybrid-electric aircraft: series, parallel, and series-parallel. A given design is classified as series when just one mechanical source of power driving the propeller (or wheels) can be recognised, whereas a parallel architecture has several sources of mechanical power. A series hybrid architecture is depicted in Figure 1. In all of the instances given, a hybrid-electric architecture is believed to be made up of batteries and ICE. [3] presented a brief outline on Electronic Devices and Circuits which forms the basis of the Clampers and Diodes..

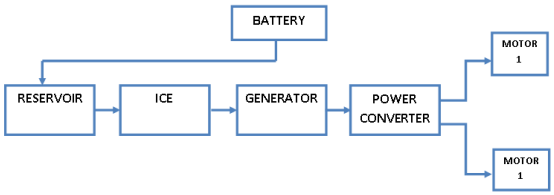

Fig 2: Series hybrid-electric architecture

A. Parallel hybrid-electric architecture

The parallel hybrid-electric architecture is more intricate than the series hybrid-electric architecture. In fact, a complicated gearbox is required to allow the propeller to be driven by both the ICE and the EM at the same time. Furthermore, the ICE is not always expected to work at its peak efficiency, but rather at a wide range of RPMs, making it less efficient in general. In contrast to series architecture, parallel architecture allows the EM to be less powerful (and, as a result, smaller and lighter) because it does not have to deliver all of the propeller's potential power on its own. The electric generator is not present since there is no need to convert ICE mechanical power to electrical power, but the benefits of doing so are outweighed by the aforementioned requirement for the complex mechanical transmission and gearbox required to transmit mechanical power between the EM,ICE, and propeller.

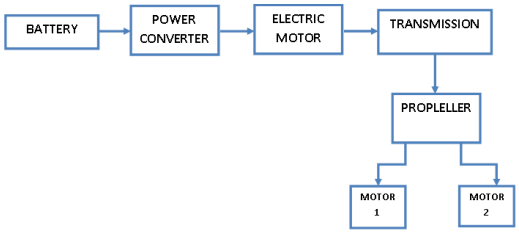

Fig 3 Parallel hybrid-electric architecture

III. BRIEF HISTORY OF ELECTRIC AIRCRAFT

The glider MB-E1 was the first human electric aircraft, tested in 1973, nearly 70 years after the Wright brothers exhibited the world's first totally controlled aero plane. The MB-electric E1's drivetrain was groundbreaking at the time. It stored energy in four Ni–Cd batteries, which provided 100 V to power a dc motor [17]. Solar cells and Ni–Cd batteries became widely available a few years later, paving the way for the first piloted solar-powered aircraft, which was demonstrated in 1979 [18]. Most of the early stage demonstrations' electrical drivetrains and aircraft constructions were not developed or optimized to integrate electrical systems; instead, they were commercially available gliders modified simply by replacing the drivetrain..

Following the first few prototypes, major advancements in the areas of solar power integration, energy storage, and lightweight structure occurred in small electric aircraft. Solar Impulse 1, a more recent attempt, exhibited an entirely solar-powered, long-range human aircraft capable of being aloft for up to 36 hours. Solar Impulse 2 covered roughly 40 000 kilometres without using any fuel in 2016..

Category	ACARE		NASA	
	Vision 2020	FlightPath 2050	N+2 (2025)	N+3 (2030–35)
Fuel	50%	75%	50%	60%
	Relative to 2000		Relative to 2005	
NO_x	80%	90%	75%	80%
	Relative to 2000		Relative to CAEP 6	
Noise	50%	65%	42 EPNdB	71 EPNdB
	Relative to 2000		Cum: relative to stage 4	

Table 1 Emission Goals Defined by ACARE Versus NASA

IV. HYBRID-E L ECT R IC AI RCRAFT S YS TEM

There are several system-level studies that compare the benefits and challenges of various architectures. Few studies measure the overall performance of one or more concept aircraft on a standard mission. [39] investigates the function of the battery system in hybrid-electric propulsion aircraft emissions, concluding that the practicality of hybrid-electric

ISSN (ONLINE): 2454-9762
ISSN (PRINT): 2454-9762
Available online at www.ijarmate.com

International Journal of Advanced Research in Management, Architecture, Technology and Engineering (IJARMATE)
Vol. 8, Issue 7, July 2022

aircraft is largely dependent on the battery system's specific energy. The simulations are based on a regional aircraft, the ATR 72, which is powered by turboprops, and the results demonstrate that hybrid architecture can be cost-competitive with a conventional system for a 350-nmi range while reducing CO2 emissions by 8%. As part of the Clean Sky 2 program, the German Aerospace Center (DLR) conducted a research that analyzed a variety of options.

The study analyzed a modelled aircraft using current technology and two versions of it to represent 2035 entry into service technology. First, the best topologies are narrowed down using a qualitative evaluation that takes into account a variety of characteristics such as aerodynamic drag, weight, system complexity, and propulsive efficiency. The parallel hybrid layout with two gas turbines and wingtip propellers with electric motors is determined to be the best contender after further quantitative examination of weight, integration, and aerodynamics. A study on the increased weight, trajectory, and range of Li–air batteries for a regional aircraft is presented in. To demonstrate how batteries affect range, the system weights for two choices are calculated and compared to a baseline of a 114 regional passenger jet with 2400nmiofrange.

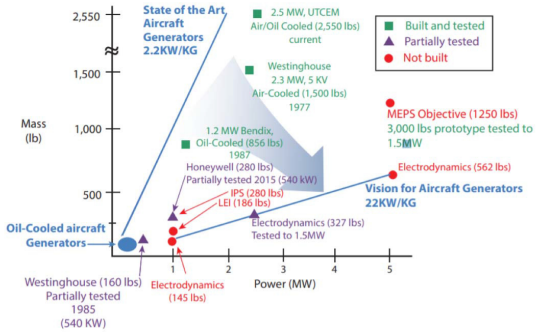

Fig 4 Analyzed current aircraft

V. PROPOSED TOPOLOGY

Power electronics is a fundamental enabling technology that enables for the efficient and effective modification of the nature of electrical energy. Controlling the voltage, current, and/or frequency of electrical energy is necessary for the management of electrical machinery as well as the generation, distribution, and storage of electrical energy aboard.The modelling and simulation of an energy efficient high power partial resonance inverter (PRI) with a matrix converter for squirrel cage induction motor drive is designed in the proposed study, with a focus on PWM modulation schemes. The PRI ensures ZVS while also lowering switching losses at the PRI's semiconductors. The matrix converter is an array of controlled semiconductor switches that links directly to the three phase source to the three phase induction motor drive because the resonant AC link has a high frequency (1.35KHz). In MATLAB/SIMULINK, the proposed concept was tested.

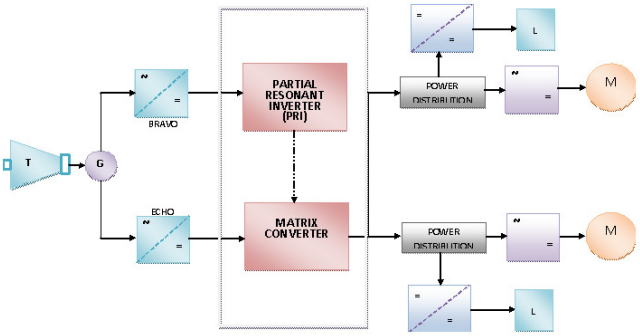

Fig 5 Block Diagram

A. *Partial Resonant Inverter*

The PRI is a single-phase inverter with a parallel resonant circuit connecting the inverter's output terminals. Figure 2 depicts the PRI's topology. The PRI's topology is comparable to that of a traditional H bridge inverter. There are also four diodes, each of which is linked to the semiconductor switches in series. In addition, unlike a regular inverter, the PRI connects the DC source across the inverter's nodes, and the resonant AC output is available across the rails.) The switching pulses obtained from the control circuit are used to switch the PRI's four power electronic switches. S1, S2, S3, and S4 IGBTs are all turned on or off at the same time.

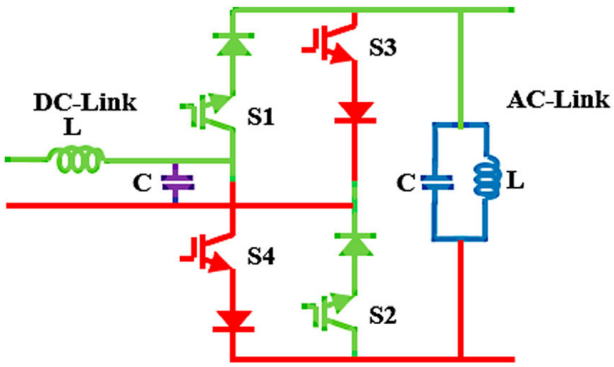

Fig 6 Topology of PRI

The switches in the same leg (S1, S4, and S3, S2) do not turn on at the same time. Figure 3 depicts the circuit layout for generating switching pulses. The modulating index can be used to alter the amplitude of the PRI's output (MI). The frequency of the AC link voltage oscillation appearing across the parallel LC circuit is given by,

L = 14mH and C = 1f, respectively. Fo = 1.35KHz by substituting the values of L and C in Equation (1). As a result, the AC link circuit is resonated at a frequency of 1.35 kHz.

The connection is allowed to swing to one of the output line voltages while in this mode. At any one time, the sum of

ISSN (ONLINE): 2454-9762
ISSN (PRINT): 2454-9762
Available online at www.ijarmate.com

International Journal of Advanced Research in Management, Architecture, Technology and Engineering (IJARMATE)
Vol. 8, Issue 7, July 2022

the output reference currents is zero. One has the greatest magnitude and is of one polarity, whereas the other two are of the opposite polarity. This simple characteristic is used by the converter to avoid any resonant swing back in the link. By discharging into two output phase pairs, the charged connection transmits power to the output. The first phase pair is made by the phase with the highest reference current and the second highest reference current, and the second phase pair is formed by the phase with the highest reference current and the lowest reference current, with the references ranked as follows:

If the output reference currents are Iao=10 A, Ibo=-7 A, and Ico=-3, phase pairings AB and AC are chosen to transfer power to the output. If V ab o and Vac o are the instantaneous voltages across these phases, and V link is the link voltage, the phase pair with the smallest voltage differential with respect to Vlink is chosen to discharge to first. If Vlink is 500 V, Vab o is 400 V, and Vac o is 300 V, the first phase pair to discharge to is AB.

B. Three phase matrix Converter

The reactive power input, on the other hand, does not have to match the reactive power output. The phase angle between the voltages and currents at the input can be modified and does not have to be the same as at the output, as previously stated. In addition, the form and frequency on both sides are independent; in other words, the input may be three-phase ac and the output could be dc, or both dc and both ac. As a result, the matrix converter topology holds promise for universal power conversion applications such as ac to dc, dc to ac, dc to dc, and ac to ac.

Compared to standard rectifier-inverter power frequency converters, the matrix converter has significant advantages.

• It has sinusoidal input and output waveforms with no sub harmonics and negligible higher order harmonics.

• Because of its intrinsic bi-directional energy flow capabilities, the input power factor is frequently completely controlled.

•Matrix converters will become more appealing when new power devices (such as silicon carbide) become available;

•Modulation control of matrix converters is not complicated.

[11] discussed about a system, a low power area reduced and speed improved serial type daisy chain memory register also known as shift Register is proposed by using modified clock generator circuit and SSASPL (Static differential Sense Amplifier based Shared Pulsed Latch). This latch based shift register consumes low area and low power than other latches. There is a modified complementary pass logic based 4 bit clock pulse generator with low power and low area is proposed that generates small clock pulses with small pulse width. These pulses are given to the conventional shift register that results high speed. The system is designed by the Cadence virtuoso 180 nm technology. The Maximum supply voltage for the system, clock source and input source are 1.8V. The complementary pass logic based proposed system reduces the area about 7% for the total system and about 23% for the 4 bit clock pulse generator circuit. The Power is reduced by 26% than the conventional system. The speed is improved about 7% than the existing system.

PWM pulse creation necessitates the use of a reference sine and triangle wave. Figure 3 shows how the reference sine wave is compared to the feedback from the output voltage, amplified, and integrated. This signal is then compared to a triangle wave that has been generated. The result of this comparison is a rectangular wave. The pulses become wider as the sine wave approaches its apex, as shown in figure 4. The duty cycle of the rectangular wave is visibly altering in accordance with the momentary value of the selected output voltage. The outcome is that the rectangular wave's effective value is the same as the output voltage. This pulse is used to control whether the power is turned on or off.

C .Space Vector Pulse Width Modulation

The spinning field of an AC machine secures the concept of space vector. During a d-q frame, three phase quantities can be turned into two phase quantities using this technique. The Park transform is used to find the d and q components, while the total power and impedance remain unaltered. Every active vector (V1 to V6) has a magnitude of 2/3 Vdc (dc bus voltage).

Fig 7

The AC machine receives the desired phase voltages through SVPWM-based converters. The duty cycle of the switches is calculated using the space vector modulation notion, which is an essential implementation of the digital control theory of PWM modulators. In comparison to traditional PWM, the space vector pulse width modulation approach has the following advantages.

A. Maximum output voltage is15.5%greater,

B. The number of switching required is about30%less

Select harmonics are injected into the sine wave to create the modulating signal. The waveform becomes flat-topped, and the amount of overmodulation is reduced. It has a higher fundamental amplitude and lower output voltage distortion. Typically, the modulating signal is made up of fundamental and harmonics.

The rotating field of an ac machine, which is utilized to modulate the converter output voltage, gives rise to the concept of space vector. The three phase quantities are frequently changed to their corresponding two phase

ISSN (ONLINE): 2454-9762
ISSN (PRINT): 2454-9762
Available online at www.ijarmate.com

quantities in this modulation technique, either in a synchronously revolving frame or in a stationary d-q frame. The magnitude of the reference vector can be determined from this two-phase component and utilized to modulate the converter output. The sinusoidal voltage is represented by SVM as a constant amplitude vector rotating at a constant frequency. This method uses a combination of the eight switching patterns to approximate the reference voltage V ref (V0toV7). The rotating vector is represented in the complex plane as illustrated in the figure.

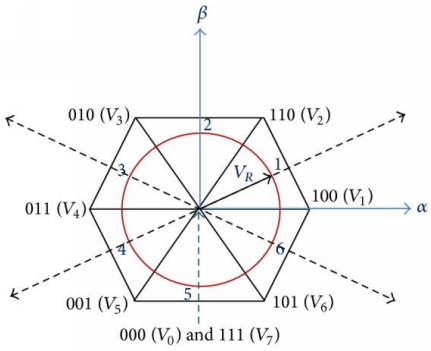

Fig 8 Rotating Vector in Complex Plane

The Pulse Width Modulation approach allows for the generation of three phase system voltages for use on the controlled output. The principle of Space Vector Modulation (SVM) differs from those of conventional PWM methods. In digital systems, implementing the SVM method takes less operation time and programmed memory. The SVM algorithm is based on the space vector u* concept, which describes all three output voltages ua, ub, and uc:

$$u^* = 2/3. (ua + a . ub + a2 .uc) \quad (1)$$

Where $a = -1/2 + j.V3/2$

Six sectors are distinguished by eight discrete vectors u0.....u7, which correspond to the 23 = 8 potential switching states of the inverter's power switches. u0 and u7 have the same amplitude of 0. The other vectors, u1 through u6, have the same amplitude but are 60 degrees offset. By adjusting the relative on-switching time Tc of the different vectors, the space vector u*, as well as the output voltages ua, ub, and uc, can be adjusted.

$$ua = Re (u^*)$$

$$ub = Re (u^*. a\text{-}1)$$

$$uc = Re (u^*.a\text{-}2)$$

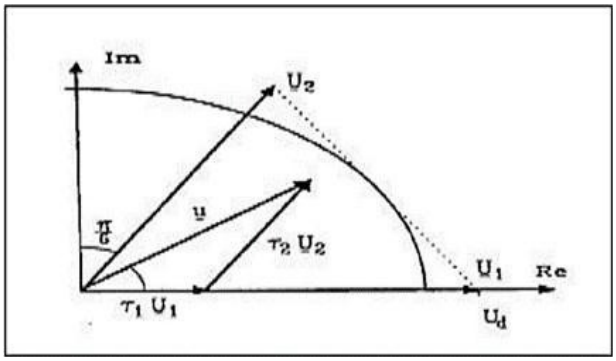

Fig 9 Switching Sequence of output voltage space vector in SVPWM technique.

ISSN (ONLINE): 2454-9762
ISSN (PRINT): 2454-9762
Available online at www.ijarmate.com

The vectors u0, u1 and u2 will be switched on alternately in the dq plane to show real and imaginary axes during a switching period Tc, taking the first sector as an example. The switching sequences of SVPWM are used to approximate the reference voltage Vref. In the modulation process, selected stationary vectors give the desired phase shift between input current and voltage, which necessitates the selection of switching vectors and the computation of vector time intervals.

The vectors shown in the SVPWM are zero vectors and active vectors. Calculating Vd,Vq,Vref, and angle () as well as the time intervals, duty cycles d,d,d0, and switching time of each IGBT switch (S1, S2, S3, S7, S8, S9) can be used to implement the SVPWM.

shaping technique in which a high frequency triangular carrier signal is compared to a sinusoidal reference signal. The fundamental benefit of carrier-based SPWM is that it has a low complexity and an excellent dynamic response for Matrix Converters, as described in the reference work "A Review of Control and Modulation Methods for Matrix Converters" by Rodriguez J, River ab M, Kolar JW, and Wheeler PW. The ratio of the triangular carrier frequency to the modulating sinusoidal frequency determines the number of pulses per cycle. The modulation ratio (MR) is calculated using the following formula:

MR = Frequency of Carrier Waveform / Frequency of the Modulating Waveform

The harmonic frequency is related to MR, and the harmonics are generally found at:

f=KMR(fm) (3),

where fm is the modulating signal's frequency and k is an integer (1, 2, 3...).

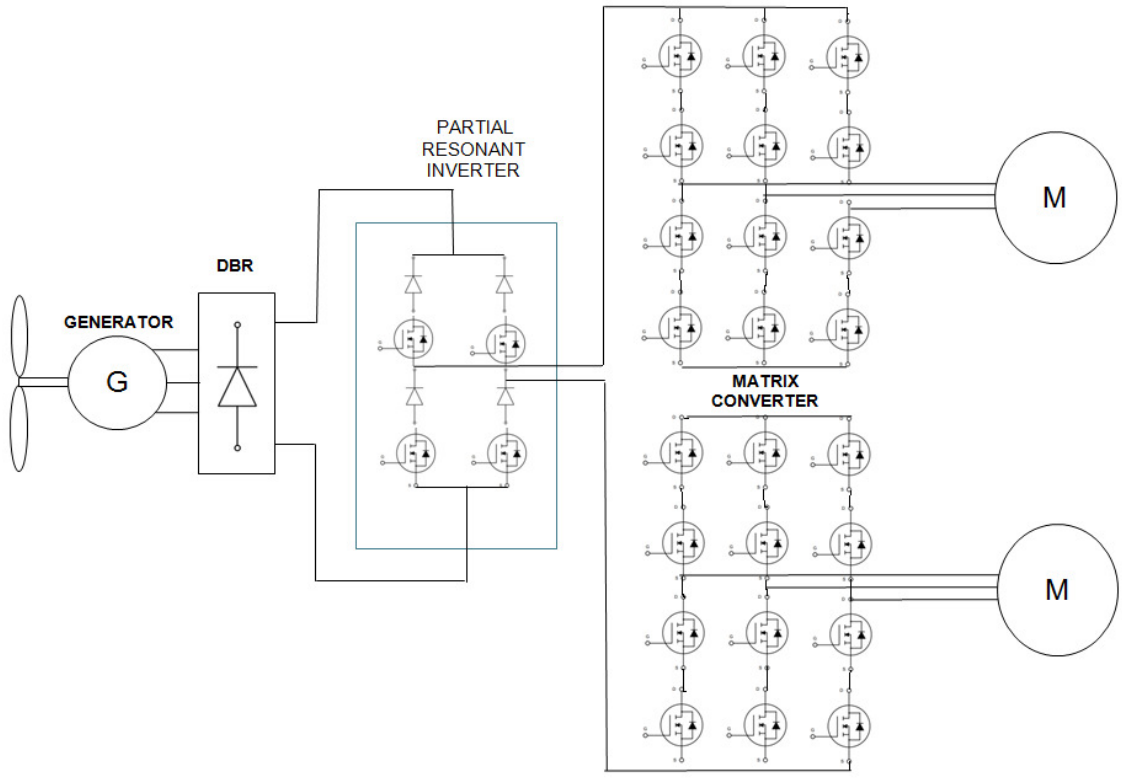

Fig 10 Proposed Topology

Sinusoidal Pulse Width Modulation Technique

The Sinusoidal Pulse Width Modulation (SPWM) technique is one of the few carrier-based modulation methods for Matrix Converter control that is straightforward. In the field of Power Electronics, the SPWM is a well-known

The modulation index (MI) is defined as the ratio of the modulating reference waveform's amplitude to the carrier waveform's amplitude, and is indicated by

MI=Ar/Ac (4)

ISSN (ONLINE): 2454-9762
ISSN (PRINT): 2454-9762
Available online at www.ijarmate.com

The reference amplitude is Ar, and the carrier amplitude is Ac. The basic (sine wave) output voltage magnitude is referred to as MI.

When MI is high, sine wave production is also high, and vice versa.

When 0 < MI < 1, the linear relationship holds: V1 = MIVin, where V1, Vin are fundamental of the output voltage and input voltage, respectively.

Induction Motor Drive

The Matrix Converter to Induction Motor Drives" is a three-phase to three-phase, ac to ac matrix converter that consists of a three-by-three switch matrix. Any input phase can be connected to any output phase at any moment thanks to the 9 bidirectional voltage blocking, current conducting switches.

For analysis, a 3x3 switch matrix can be organized in the form of Fig. 8. Because an inductive load is anticipated, the input voltage sources must be established by connecting the converter input phases with capacitors (filters). Figure 8 also shows the main power source's impedance, or leakage inductance 1, as well as the resistance r. In theory, by toggling the matrix switches appropriately for a given set of input three phase voltages, any desired set of output voltages can be produced.

Figure 8 also shows how the required bi-directional switch can be implemented using a back-to-back arrangement of IGBTs. The reverse voltage blocking capability is provided by the two diodes. By using the short at the midpoint of the two branches, the diodes are effectively arranged in parallel with the IGBT. The matrix converter in Fig.8 requires a total of 18 sets of an IGBT and a diode to be implemented.

This setup is preferred to equivalent configurations without a mid-point short because it prevents the IGBTs from avalanching during the cessation of the reverse current. Furthermore, because the common collector arrangement requires the fewest number of isolated gate drives, namely 6, this switch configuration is the most cost-effective and technically desirable of all back-to-back IGBT layouts.

When comparing the number of semiconductors required, the matrix converter requires 6 more IGBTs and 6 more diodes than the similar PWM dc-voltage-link converter when the design depicted in Fig.8 is adopted. Despite the different numbers of required semiconductors, a detailed examination of the switch ratings reported in this paper reveals that the installed total switch power of both circuits is roughly the same due to the possibility of a one-third reduction in the current ratings of the matrix converter switches.

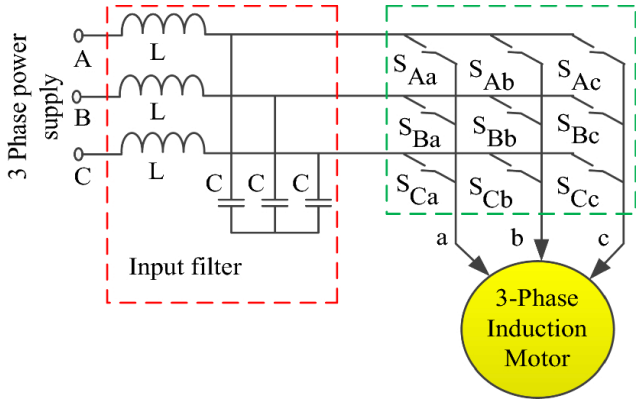

Fig 11 3 phase Matrix converter

The cost of semiconductors can be further decreased by utilizing NPT-IGBTs' ability to block both forward and reverse voltages. When compared to a dc voltage link converter, the deletion of series diodes and probable reductions in IGBT current ratings could significantly reduce the matrix converter's installed total switch power.

A drive setup for field oriented control of an induction motor driven by a three phase to three phase matrix converter is shown in the figure. The angular position of rotor 0 is determined using an incremental encoder or resolver. To form the angular position of the stator MMF 0, the angular position of the slip e, which is determined in the field oriented control module, is added to the angular position of the rotor 0. The physical stator currents are referred from the physical (stationary) reference frame to the synchronously rotating(d-q)axes using these sinusoidal components. Speed is also measured using the encoder. The field oriented controller's voltage command signals are routed into the matrix converter block, which generates three phase PWM voltage pulses to drive the induction motor. Filters on the input side complete the 3 phase to 3 phase matrix converter. In motor drive applications, where the stator winding inductances of the motor act as filters, the output side filters can usually be eliminated.

The filters on the input side play a vital role in preventing the input voltage from fluctuating greatly during each PWM cycle.

Another significant function is to absorb harmonic currents generated by matrix converters in order to prevent undesirable harmonic currents from entering into ac main supply and to comply with any applicable power quality regulation. Figure 8 shows a simple filter arrangement with a capacitor linked between each line and line at the matrix converter input..

ISSN (ONLINE): 2454-9762
ISSN (PRINT): 2454-9762
Available online at www.ijarmate.com

International Journal of Advanced Research in Management, Architecture, Technology and Engineering (IJARMATE)
Vol. 8, Issue 7, July 2022

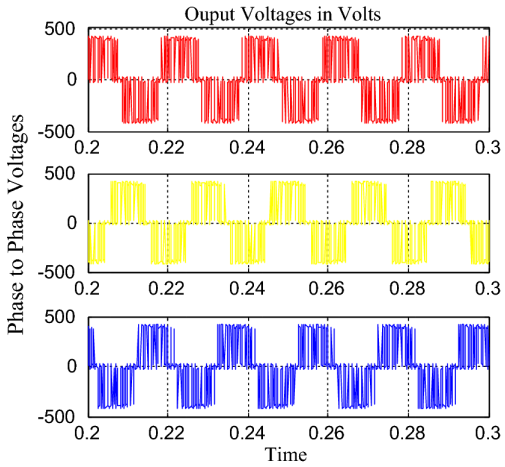

Fig 12 Induction Motor Phase voltage

Selective Harmonic Elimination

Only half of the angles 1, 2, 3, etc. must be found in selective harmonic elimination because of the voltage wave's quarter-wave symmetry. Equation (6) is determined after analysing the Fourier series expansion to determine the firing angles..

$$H_n = \frac{4Vdc}{n\pi}\sum_{i=1}^{k}[\cos(\alpha_i)]$$

k is the number of switching angles, n is the odd harmonics, and I is the switching angle that needs to be computed, where Hn is the output wave's Fourier function, Vdc is the DC power supply's voltage, and k is the number of switching angles. The switching angles need to adhere to the restrictions.

Modelling of Wind Turbine

When using a wind energy conversion system, wind energy is first converted to mechanical energy in the turbine and then to electrical energy in the generator. However, the amount of electrical energy produced only depends on the wind speed impacting the turbine's blade. Additionally, the output's stability is influenced by the tip speed ratio (), pitch angle (), and wind speed (V) The wind energy that is available can be stated as,

$$P_{out} = C0.5\rho_w A_S V^3$$

$$P_{out} \propto 0.5\rho_w A_S V^3$$

where,

Pout is available wind power (Watt).

ρw is the moving air density (Kg/m3

AS is the Swept area by the blade (m2).

V is the wind velocity (m/s).

C is the power coefficient, which depend on the tip speed ratio and pitch angle.

The torque developed in the turbine can be stated as,

$$T_w = P_{out}/\omega_{rotor}$$

where,

Tw = Torque developed.

ωrotor = Rotor speed (rad/sec).

The power coefficient is given by,

$$C(\lambda,\beta) = 0.73\left(151\lambda i - 0.58\beta - 0.002\beta^{2.14} - 13.2\right)e^{-18.4\lambda i}$$

where,

$$\lambda i = 1.1\lambda + 0.02\beta - 0.03\beta^3 + 1$$

λ is given by,

$$\lambda = \omega_{rotor} R/V$$

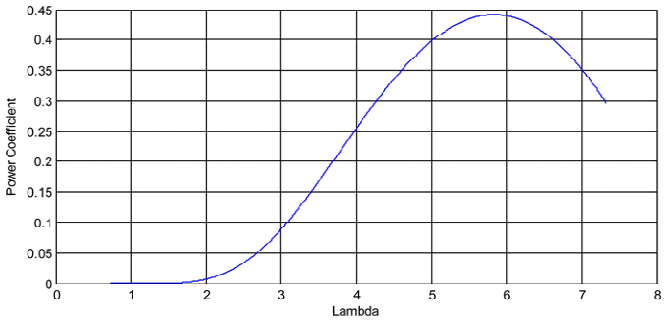

Fig 13 **Coefficient of power with tip speed ratio**

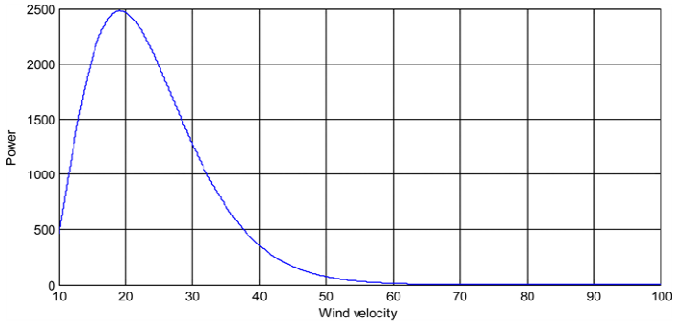

Fig 14 **Output power from turbine with wind speed**

ISSN (ONLINE): 2454-9762
ISSN (PRINT): 2454-9762
Available online at www.ijarmate.com

International Journal of Advanced Research in Management, Architecture, Technology and Engineering (IJARMATE)
Vol. 8, Issue 7, July 2022

Energy Storage

The current state-of-the-art energy storage systems utilize Li-ion batteries that had been established for decades. However, one of the biggest obstacles to commercial-scale all-electric aircraft continues to be the unique energy constraints of Li-ion batteries. Today's top Li-ion battery has a specific energy of roughly 250 Wh/kg. The specific energy of jet fuel, which is 12 000 Wh/kg, much outperforms this.

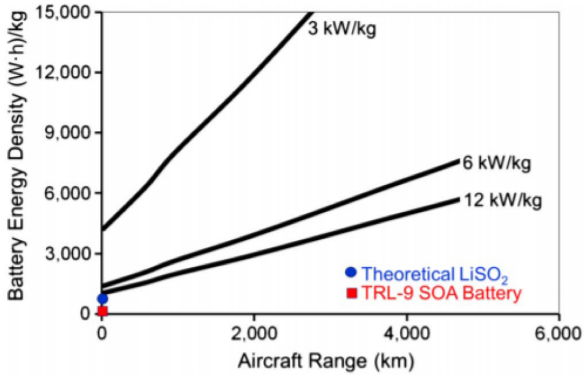

Fig 15 Usable battery energy density needed versus range for a single-aisle airliner

[14] proposed a system which can achieve a higher throughput and higher energy efficiency. The S-BOX is designed by using Advanced Encryption Standard (AES). The AES is a symmetric key standard for encryption and decryption of blocks of data. In encryption, the AES accepts a plaintext input, which is limited to 128 bits, and a key that can be specified to be 128 bits to generate the Cipher text. In decryption, the cipher text is converted to original one. By using this AES technique the original text is highly secured and the information is not broken by the intruder. From that, the design of S-BOX is used to protect the message and also achieve a high throughput, high energy efficiency and occupy less area.

A cell with 300 Wh/kg was shown to be capable of eight cycles. The Li–S battery is another option for the next-generation battery. A target for specific power above 500 Wh/kg at the cell level is set by the U.K.-based company Ox is Energy. However, Li–S batteries may face difficulties such as cathode deterioration and overheating. Despite the difficulties, 500 cycles are anticipated, which is within the range of the existing Li-ion batteries.

[9] proposed a system, this paper presents an effective field programmable gate array (FPGA)-based hardware implementation of a parallel key searching system for the brute-force attack on RC4 encryption. The design employs several novel key scheduling techniques to minimize the total number of cycles for each key search and uses on-chip memories of the FPGA to maximize the number of key searching units per chip. Based on the design, a total of 176 RC4 key searching units can be implemented in a single Xilinx XC2VP20-5 FPGA chip. Operating at a 47-MHz clock rate, the design can achieve a key searching speed of 1.07 x 107 keys per second. Breaking a 40-bit RC4 encryption only requires around 28.5 h.

The range of all-electric flight is limited until solutions and technological advancements are found because energy storage density is a critical aspect in the long-term adoption of electrical aircraft propulsion systems.

Electric Machines

As illustrated in Table 4, a NASA assessment that assesses the essential technologies for electric aircraft compares the most advanced mechanical energy conversion between internal combustion engines (ICE), electric motors, and gas turbines. The document presents key factors to take into account when choosing the best motor type for more-electric aircraft (MEA). The main criteria for electric machines used in aero planes are identified as being weight, volume, dependability, efficiency, and cost. These criteria, which include the cause of losses, thermal and mechanical rotor restrictions, torque ripple, short-circuit behavior, and power density, are qualitatively assessed for existing conventional motor types.

Even though their short-circuit behavior is subpar compared to that of an induction or reluctance machine and necessitates the use of proper system architecture and controls, PM slot less multipole machines are noted as being the best overall in the final review. Although this work focuses on no propulsion applications, high-power propulsion machines can still face significant difficulties. The following is the general formula for sizing electric machines:

$$P = k \quad AB(D2L)N$$

where D is the diameter, L is the stack length, N is the rotational speed, k is a constant for geometry and motor type, is the efficiency, A is the linear current density, B is the airgap flux density, and D is the diameter. Due to cooling issues and material constraints, current density and airgap flux density are physically constrained in this situation, supporting the conventional wisdom that machines are sized for torque and that the simplest way to increase the power density of a machine is to increase its operating speed. The machine's weight exhibits a similar pattern to the volume as indicated by D2L. The rotor must work harder to maintain structural and dynamic stability as operating speed increases.

Type / efficiency	Commercial product	Power (kW) / efficiency	Specific power (kW/kg)
ICE (30%)	Continental IO-550	224 kW	0.984
	Rotax 912	74.6 kW	1.10
Electric motors (95%)	Tesla automobile	182	3.49
	Honda FCX	100	2.96
Gas turbine (34%)	P&W PT6A	1125	5.1

ISSN (ONLINE): 2454-9762
ISSN (PRINT): 2454-9762
Available online at www.ijarmate.com

International Journal of Advanced Research in Management, Architecture, Technology and Engineering (IJARMATE)
Vol. 8, Issue 7, July 2022

Table 2 Efficiency of hybrid vehicles

It is summarized as a particular power vs speed plot. High specific power in electrical equipment may be made possible by faster speeds, as previously mentioned. However, this plot implies that this is not accomplished in practice at reasonably high speeds since it contains a wide range of machines with various power levels.

Power density may be compromised by high-frequency effects. For instance, high core losses might necessitate lowering the magnetic loadings. To maintain high torque density at high speeds, new machine architectures, such as slot-less machines, are being developed.

In Fig. 9, the identical data are converted to specific power vs power. Zhang et al. pinpoint a few causes for decreasing specific power with rising power, even though the pattern cannot be clearly seen with the available data. Since the volume of the machine does not rise correspondingly to the power, the electromagnetic loading in the machine must be reduced with rising power to accept the same loss density. Second, because of the greater stresses in the structure caused by the higher speed designs, more structural weight is needed. Third, because the majority of high specific power machines require extensive cooling, their weight is increased.

[5] proposed a system, Low Voltage Differential Signaling (LVDS) is a way to communicate data using a very low voltage swing (about 350mV) differentially over two PCB traces. It deals about the analysis and design of a low power, low noise and high speed comparator for a high performance Low Voltage Differential Signaling (LVDS) Receiver. The circuit of a Conventional Double Tail Latch Type Comparator is modified for the purpose of low-power and low noise operation even in small supply voltages. The circuit is simulated with 2V DC supply voltage, 350mV 500MHz sinusoidal input and 1GHz clock frequency.

Physical restrictions are present in conventional motors, despite current development efforts pushing for additional increases in specific power. It has been shown that cryogenic machines can deliver substantially higher specific power than traditional (noncryogenic) machines. As a result, interest in partially or entirely superconducting (cryogenic) equipment is growing as well. HTS coil-based partially superconducting machines have been demonstrated in the past at various speeds and power levels. The HTS coils are a desirable option for electric aircraft propulsion because to their increased electrical and magnetic loadings.

A homopolar machine with a specific power of above 9 kW/kg, including the weight of the cryogenic cooling system, and a net efficiency above 96% is constructed and tested utilising HTS coils, as reported in. In order to obtain a specific power exceeding 16 kW/kg, a machine design created by NASA with an incorporated spinning cryocooler is presented in. Future designs and machine technology must take the power density into consideration because electrical machines are a crucial part of the electrical drivetrain.

Simulation and experimental results

The simulation diagram for the suggested system is shown in the Figure. Along with the DBRs, high-frequency transformers with two isolated secondary windings are also exhibited. Table displays the simulation's input parameters. Figure displays the PRI's Simulink model. It is demonstrated that the switching pulses for the PRI are produced with a fixed modulation index of 0.45. The H Bridge handling the increased voltage has a 210V DC link voltage.

The squirrel cage induction machine rotates at 1750 rpm, which is its nominal speed. A speed change from zero to nominal speed followed by a decrease in speed to 780 rpm is taken into consideration as a case study. Fig. 8 depicts the reference motor speed and the actual motor speed.

As it can be seen the motor speed can follow its reference and the error is very small.

The load torque for this case study is 15 Nm, as shown in Fig. 9. When the machine is running at 1750 rpm, Fig. 10 shows the stator current (the converter's output current) and voltage. Fig. 11 shows the current and voltage of phase "a" at the converter's input side when the induction machine is spinning at 1750 rpm. The input current has an amplitude of 20 A. This figure makes it evident that the input current and voltage are in phase. As a result, no additional power factor correction module is needed. Fig. shows the stator current and voltage in the instance when the machine speed is 780 rpm. The stator frequency in this instance is 28 Hz. The link voltage and current are depicted in Figs and 14, respectively.

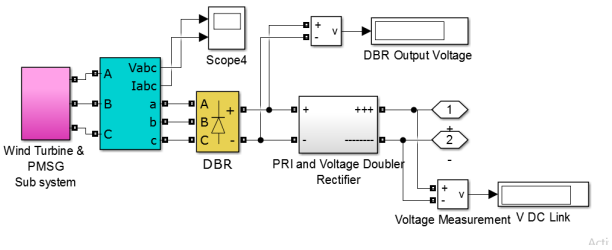

Fig 16 Simulation diagram of the proposed system

The switching pulses for switching modules Y1, Y2, Y3, and Y4 are shown in the figures. A 400V AC link voltage causes the AC link to resonate at a frequency of 1.35KHz. Information about the AC link voltage's partial resonance is

ISSN (ONLINE): 2454-9762
ISSN (PRINT): 2454-9762
Available online at www.ijarmate.com

International Journal of Advanced Research in Management, Architecture, Technology and Engineering (IJARMATE)
Vol. 8, Issue 7, July 2022

showninFigure15.

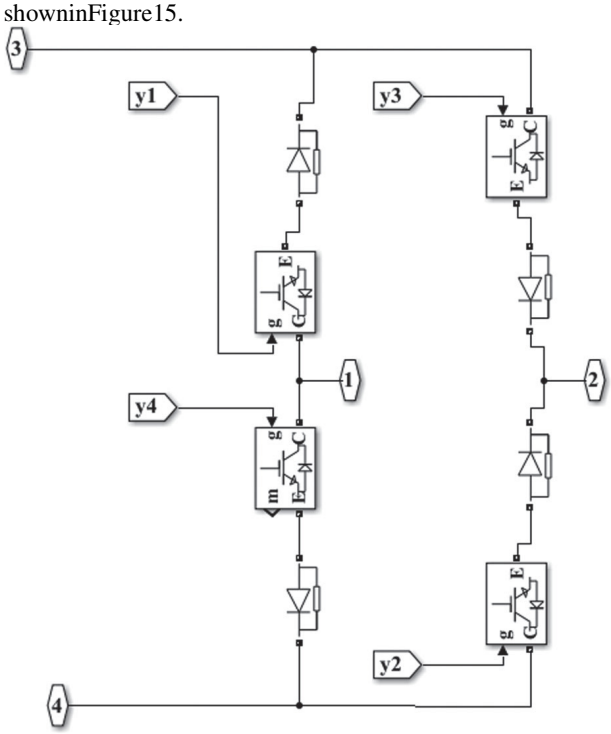

Fig 17 Simulink model of PRI

The resonant AC bus bar is used to generate the two isolated DC voltages. The primary of each of the two ferrite core transformers is linked across the resonant AC bus bar. The filter capacitors used after the rectifiers are also small since the AC link resonates at a frequency of over 1.35KHz.

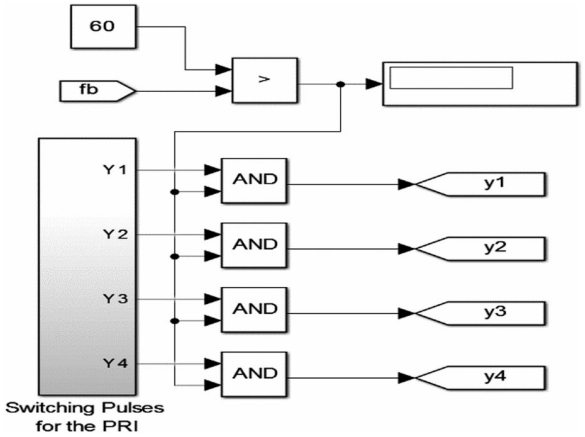

Fig 18 Switching Pulses for PRI.

The function of matrix converter is creating the switching functions of the bidirectional switches. These functions are gate drive signals of the power switches in real converter

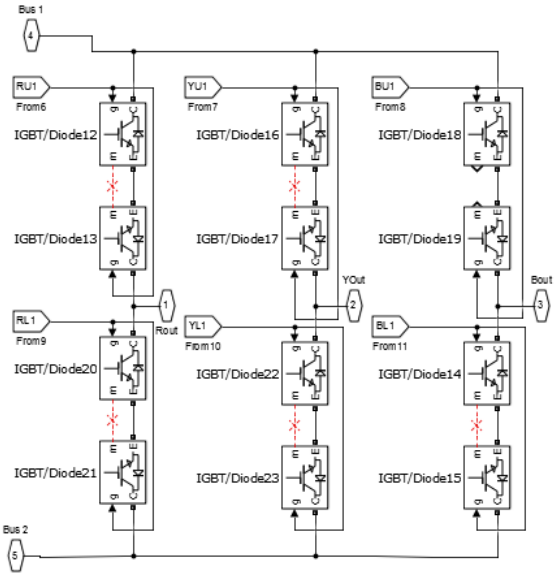

Fig 19 Matrix Converter

A matrix converter can be used to generate bi-directional power flow, and by properly managing the switching devices, both the output voltage and the input current can be sinusoidal. This is only accurate provided the load does not experience power fluctuations that would be fed to the input supply and cause a distortion in the line currents. This is a significant issue which has been taken into consideration while looking at the qualities of the application to be implemented.

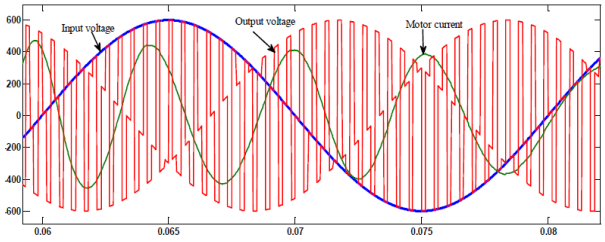

Fig 20 Waveforms for input voltage, output current and motor

Another important role is to absorb harmonic currents, which are generated by matrix converters, to prevent unwanted harmonic currents from flowing into ac main supplies and to satisfy any power quality regulation applicable. A simple filter configuration was examined, as shown, where a capacitor is connected between each line to line at the matrix converter input. The 3 phase to 3 phase matrix converter is completed by filters at the input side. The output side filters can generally be omitted in motor drive applications, where the stator winding inductances of the motor work as the filters. One important role of the filters at input side is to keep the input voltage from changing significantly during each PWM cycle.

ISSN (ONLINE): 2454-9762
ISSN (PRINT): 2454-9762
Available online at www.ijarmate.com

International Journal of Advanced Research in Management, Architecture, Technology and Engineering (IJARMATE)
Vol. 8, Issue 7, July 2022

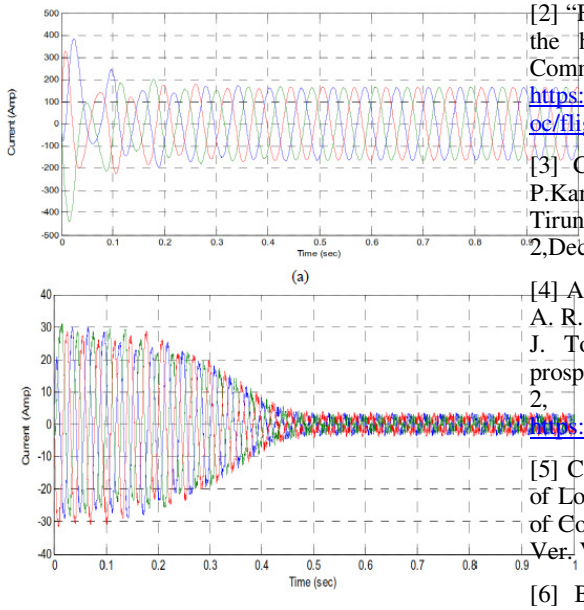

Fig 21 **simulation results (a) matrix converter only, (b) with IM.**

Conclusion

The era of electrified propulsion in large aircraft may not be far off, as evidenced by recent technological advancements and the united efforts of governments and business. The technology roadmaps for the sector support this. Along with the availability of the enabling technology, there are significant obstacles that still need to be overcome, such as guaranteeing safety, developing a certification pathway, and integrating the technology into platforms for commercial aero planes. This fascinating use of electrical technology is becoming a reality thanks in large part to the flight demonstrations being conducted with hybrid and all-electric aircraft, including regional aircraft platforms. This article suggests a hybrid control technique for a squirrel cage induction motor drive fed by a matrix converter.

A revised control structure using a vector modulation strategy has been devised after several modulation strategies for the control of the matrix converter have been simulated. The voltage transfer ratio is better than with the older control approaches, according to the simulation data. Additionally, the suggested system reduces the harmonics of the current and voltage. The topology is projected to deliver relatively low cost, low weight, compact and efficient power converters and motor drives.

REFERENCE

[1] S. Øvrebø, S. Tiwari, and S. Skaar, "Test and Validation of the Mark 1 (2.5 MW) E-Fan X Generator," in Proc. NATO AVT-RSY-323 Research Symp. Hybrid/Electric Aero-Propulsion Syst. for Military Appl. (Session: Integrated Power-train 2), Oct 2019.

[2] "Flightpath 2050: Europe's vision for aviation - report of the high level group on aviation research," European Commission, no. https://ec.europa.eu/transport/sites/transport/files/modes/air/doc/flightpath2050.pdf, 2011.

[3] Christo Ananth, S.Esakki Rajavel, S.Allwin Devaraj, P.Kannan. "Electronic Devices.", ACES Publishers, Tirunelveli, India, ISBN: 978-81-910-747-6-5, Volume 2,December 2014, pp:1-300.

[4] A. W. Schäfer, S. R. H. Barrett, K. Doyme, L. M. Dray, A. R. Gnadt, R. Self, A. O'Sullivan, A. P. Synodinos, and A. J. Torija, "Technological, economic and environmental prospects of all-electric aircraft," Nature Energy, vol. 4, no. 2, pp. 160–166, 2019. [Online]. Available: https://doi.org/10.1038/s41560-018-0294-x

[5] Christo Ananth, Bincy P Chacko, "Analysis and Design of Low Voltage Low Noise LVDS Receiver", IOSR Journal of Computer Engineering (IOSR-JCE), Volume 9, Issue 2, Ver. V (Mar - Apr. 2014), PP 10-18.

[6] B. S. Bhangu and K. Rajashekara, "Electric starter generators: Their integration into gas turbine engines," IEEE Ind. Appl. Mag., vol. 20, no. 2, pp. 14–22, March 2014.

[7] M. Lukic, P. Giangrande, A. Hebala, S. Nuzzo, and M. Galea, "Review, challenges, and future developments of electric taxiing systems," IEEE Trans. Transport. Electrific., vol. 5, no. 4, pp. 1441–1457, Dec 2019.

[8] E. D. Ganev, "Electric drives for electric green taxiing systems: Examining and evaluating the electric drive system," IEEE Electrif. Mag., vol. 5, no. 4, pp. 10–24, Dec 2017.

[9] Christo Ananth, Muthamil Jothi.M, M.Priya, V.Manjula, "Parallel RC4 Key Searching System Based on FPGA", International Journal of Advanced Research in Management, Architecture, Technology and Engineering (IJARMATE), Volume 2, Special Issue 13, March 2016, pp: 5-12.

[10] S. Wang, S. Zhang, and S. Ma, "An energy efficiency optimization method for fixed pitch propeller electric aircraft propulsion systems," IEEE Access, vol. 7, pp. 159 986–159 993, 2019.

[11] Christo Ananth, S. Dinesh, "Area power and speed optimized serial type daisy chain memory using modified CPG with SSASPL," 2015 International Conference on Control, Instrumentation, Communication and Computational Technologies (ICCICCT), Kumaracoil, India, 2015, pp. 344-349,IEEE Data retrieved from http://ieeexplore.ieee.org/stamp/stamp.jsp?tp=&arnumber=7475302&isnumber=7475237.

[12] M. Hirst, A. Mcloughlin, P. J. Norman, and S. J. Galloway, "Demonstrating the more electric engine: a step towards the power optimised aircraft," IET Electr. Power Appl., vol. 5, no. 1, pp. 3–13, January 2011.

ISSN (ONLINE): 2454-9762
ISSN (PRINT): 2454-9762
Available online at www.ijarmate.com

International Journal of Advanced Research in Management, Architecture, Technology and Engineering (IJARMATE)
Vol. 8, Issue 7, July 2022

[13] K. Rajashekara, "Parallel between more electric aircraft and electric/ hybrid vehicle power conversion technologies," IEEE Electrific. Mag., vol. 2, no. 2, pp. 50–60, June 2014.

[14] Christo Ananth, H. Anusuya Baby, "S-Box using AES Technique", International Journal of Engineering Research & Technology (IJERT), Vol. 3 Issue 3, March – 2014, pp 285-290.

[15] M. Galea, P. Giangrande, V. Madonna, and G. Buticchi, "Reliabilityoriented design of electrical machines: The design process for machines' insulation systems must evolve," IEEE Ind. Electron. Mag., vol. 14, no. 1, pp. 20–28, 2020.

[16] F. Bu, H. Liu, W. Huang, Y. Hu, M. Degano, C. Gerada, and K. Rajashekara, "Induction-machine-based starter/generator systems: Techniques, developments, and advances," IEEE Ind. Electron. Mag., vol. 14, no. 1, pp. 4–19, 2020.

[17] J. Chen, Q. Song, S. Yin, and J. Chen, "On the decentralized energy management strategy for the all-electric apu of future more electric aircraft composed of multiple fuel cells and supercapacitors," IEEE Trans. Ind. Electron., 2019.

[18] Y. Zhang, Y. Yu, R. Su, and J. Chen, "Power scheduling in more electric aircraft based on an optimal adaptive control strategy," IEEE Trans. Ind. Electron., 2019.

[19] M. Flynn, M. Sztykiel, C. E. Jones, P. J. Norman, G. M. Burt, P. Miller, and M. Husband, "Protection and fault management strategy maps for future electrical propulsion aircraft," IEEE Trans. Transport. Electrific., vol. 5, no. 4, pp. 1458–1469, 2019.

[20] W. Cao, B. C. Mecrow, G. J. Atkinson, J.W. Bennett, and D. J. Atkinson, "Overview of electric motor technologies used for more electric aircraft (mea)," IEEE Trans. Ind. Electron., vol. 59, no. 9, pp. 3523–3531, Sep. 2012.

[21] Y. Wang, S. Nuzzo, H. Zhang, W. Zhao, C. Gerada, and M. Galea, "Challenges and opportunities for wound field synchronous generators in future more electric aircraft," IEEE Trans. Transport. Electrific., 2020.

[22] M. E. Elbuluk and M. D. Kankam, "Potential starter/generator technology for future aerospace application," IEEE Aerosp. Electron. Syst. Mag., vol. 11, no. 10, pp. 17–24, Oct 1996.

[23] V. Madonna, P. Giangrande, L. Lusuardi, A. Cavallini, C. Gerada, and M. Galea, "Thermal overload and insulation aging of short duty cycle, aerospace motors," IEEE Trans. Ind. Electron., pp. 1–1, 2019.

[24] V. Madonna, P. Giangrande, C. Gerada, and M. Galea, "Thermal analysis of fault-tolerant electrical machines for more electric aircraft applications," JOE, vol. 2018, no. 13, pp. 461–467, 2018.

[25] V. Madonna, A. Walker, P. Giangrande, G. Serra, C. Gerada, and M. Galea, "Improved thermal management and analysis for stator endwindings of electrical machines," IEEE Trans. Ind. Electron., vol. 66, no. 7, pp. 5057–5069, July 2019.

[26] Z. Song, C. Liu, K. Feng, H. Zhao, and J. Yu, "Field prediction and validation of a slotless segmented-halbach permanent magnet synchronous machine for more electric aircraft," IEEE Trans. Transport. Electrific., pp. 1–1, 2020.

[27] M. Mazzoleni, F. Previdi, M. Scandella, and G. Pispola, "Experimental development of a health monitoring method for electro-mechanical actuators of flight control primary surfaces in more electric aircrafts," IEEE Access, vol. 7, pp. 153 618–153 634, 2019.

[28] V. Madonna, P. Giangrande, and M. Galea, "Electrical power generation in aircraft: Review, challenges, and opportunities," IEEE Trans. Transp. Electrific., vol. 4, no. 3, pp. 646–659, Sep. 2018.

[29] J. Chen, C. Wang, and J. Chen, "Investigation on the selection of electric power system architecture for future more electric aircraft," IEEE Trans. Transport. Electrific., vol. 4, no. 2, pp. 563–576, June 2018.

[30] B. Rahrovi and M. Ehsani, "A review of the more electric aircraft power electronics," in Proc. IEEE Texas Power and Energy Conf. (TPEC), Feb 2019, pp. 1–6.

[31] G. Buticchi, S. Bozhko, M. Liserre, P. Wheeler, and K. Al-Haddad, "On-board microgrids for the more electric aircraft—technology review," IEEE Trans. Ind. Electron., vol. 66, no. 7, pp. 5588–5599, July 2019.

[32] K. Ni, Y. Liu, Z. Mei, T.Wu, Y. Hu, H.Wen, and Y.Wang, "Electrical and electronic technologies in more-electric aircraft: A review," IEEE Access, vol. 7, pp. 76 145–76 166, 2019.

[33] J. Chen, Y. Shen, J. Chen, H. Bai, C. Gong, and F. Wang, "Evaluation on the auto-configured multi-pulse ac/dc rectifiers and their application in more electric aircrafts," IEEE Trans. Transport. Electrific., 2020.

[34] J. Benzaquen and B. Mirafzal, "Seamless dynamics for wild-frequency active rectifiers in more electric aircraft," IEEE Trans. Ind. Electron., 2019.

[35] Z. Dai, J. Yang, D. Rao, J. Zhang, and Z. Zhang, "A global convergence estimator of grid voltage parameters for more electric aircraft," IEEE Trans. Ind. Electron., pp. 1–1, 2019.

[36] Y. Zhang, J. Xia, X. Zhang, Z. Chen, B. Li, Q. Luo, and Y. He, "Modeling and prediction of the reliability analysis of an 18-pulse rectifier power supply for aircraft based applications," IEEE Access, vol. 8, pp. 47 063– 47 071, 2020.

[37] J. Benzaquen, F. Fateh, M. B. Shadmand, and B. Mirafzal, "Performance comparison of active rectifier control schemes in more electric aircraft applications," IEEE Trans Transport. Electrific., vol. 5, no. 4, pp. 1470– 1479, 2019.

[38] G. Buticchi, L. Costa, and M. Liserre, "Improving system efficiency for the more electric aircraft: A look at

ISSN (ONLINE): 2454-9762
ISSN (PRINT): 2454-9762
Available online at www.ijarmate.com

International Journal of Advanced Research in Management, Architecture, Technology and Engineering (IJARMATE)
Vol. 8, Issue 7, July 2022

dcdc converters for the avionic onboard dc microgrid," IEEE Ind. Electron. Mag., vol. 11, no. 3, pp. 26–36, 2017.

[39] I. Moir and A. Seabridge, Aircraft Systems: Mechanical, electrical, and avionics subsystems integration. John Wiley & Sons, 2011, vol. 52.

[40] S. Yin, K. J. Tseng, R. Simanjorang, Y. Liu, and J. Pou, "A 50-kw highfrequency and high-efficiency sic voltage source inverter for more electric aircraft," IEEE Trans. Ind. Electron., vol. 64, no. 11, pp. 9124–9134, 2017.

[41] R. Rui and I. Cotton, "Impact of low pressure aerospace environment on machine winding insulation," in Proc. IEEE Int. Symp. Electr. Insul. IEEE, 2010, pp. 1–5.

[42] Y. Wang, T. Balachandran, Y. Hoole, Y. Yin, and K. S. Haran, "Partial discharge investigation of form-wound electric machine winding for electric aircraft propulsion," IEEE Trans. Transport. Electrific., 2020.

[43] H. Schefer, L. Fauth, T. H. Kopp, R. Mallwitz, J. Friebe, and M. Kurrat, "Discussion on electric power supply systems for all electric aircraft," IEEE Access, vol. 8, pp. 84 188–84 216, 2020.

[44] V. Madonna, P. Giangrande, W. Zhao, H. Zhang, C. Gerada, and M. Galea, "On the design of partial discharge-free low voltage electrical machines," in Proc. IEEE Int. Electr. Mach. Drives Conf. (IEMDC), 2019, pp. 1837–1842.

[45] J. Wei, H. Xu, B. Zhou, Z. Zhang, and C. Gerada, "An integrated method for three-phase ac excitation and high-frequency voltage signal injection for sensorless starting of aircraft starter/generator," IEEE Trans. Ind. Electron., vol. 66, no. 7, pp. 5611–5622, July 2019.

[46] A. Griffo, D. Drury, T. Sawata, and P. H. Mellor, "Sensorless starting of a wound-field synchronous starter/generator for aerospace applications," IEEE Trans. Ind. Electron., vol. 59, no. 9, pp. 3579–3587, Sep. 2012.

[47] D. Golovanov, L. Papini, D. Gerada, Z. Xu, and C. Gerada, "Multidomain optimization of high-power-density pm electrical machines for system architecture selection," IEEE Trans. Ind. Electron., vol. 65, no. 7, pp. 5302–5312, 2018.

[48] Y. Zhang, S. McLoone, W. Cao, F. Qiu, and C. Gerada, "Power loss and thermal analysis of a mw high-speed permanent magnet synchronous machine," IEEE Trans. Energy Convers., vol. 32, no. 4, pp. 1468–1478, 2017.

[49] A. Yoon, Xuan Yi, J. Martin, Yuanshan Chen, and K. Haran, "A highspeed, high-frequency, air-core pm machine for aircraft application," in Proc. IEEE Power Energy Conf. Illinois, 2016, pp. 1–4.

[50] A. D. Anderson, Y. Wang, Y. Yu, and K. S. Haran, "Experimental validation of a high-power slotless stator," in Proc. IEEE Int. Electr. Mach. Drives Conf., 2019, pp. 1564–1569.

[51] R. Van Millingen and J. van Millingen, "Phase shift torquemeters for gas turbine development and monitoring," in Proc. ASME Int. Gas Turb. Aeroeng. Congr. Expo. American Society of Mechanical Engineers Digital Collection, 1991.

[52] C. P. Mudannayake and M. F. Rahman, "Control design for an inductions machine based 42v integrated starter alternator," IEEE Ind. Appl. Mag., vol. 15, no. 4, pp. 14–25, 2009.

[53] "Rolls Royce - For the development of the Embedded Electrical Starter Generator (E2SG)," IOP Institute of Physics: https://www.iop.org/activity/business/innovation/2017-winners/commended-innovation/rollsoyce/page70258:htmlgref; 2020:

[54] J. Seo, S. Kim, and H. Jung, "Rotor-design strategy of ipmsm for 42 v integrated starter generator," IEEE Trans. Magn., vol. 46, no. 6, pp. 2458–2461, 2010.